Optimizing MR imaging for detecting small tumors in the cerebellopontine angle and internal auditory canal.

D R Enzmann and J O'Donohue

AJNR Am J Neuroradiol 1987, 8 (1) 99-106
http://www.ajnr.org/content/8/1/99

Optimizing MR Imaging for Detecting Small Tumors in the Cerebellopontine Angle and Internal Auditory Canal

Dieter R. Enzmann
Jim O'Donohue

Relative resolving power was used to determine the optimal MR imaging pulse sequence for detecting small tumors of the internal auditory canal and the cerebellopontine angle. Resolving power takes into consideration these important image characteristics: signal-to-noise ratio, contrast, and spatial resolution. The study was performed on a 1.5-T magnet using a 256 × 256 matrix and a 3-mm slice thickness. The TR ranged from 400–2000 msec; the number of excitations was either two or six; and the pixel size was 0.94, 0.78, or 0.63 mm. Theoretical calculations of relative resolving power were compared with the relative resolving power of 45 control patients and 15 patients with small tumors of the cerebellopontine angle or internal auditory canal. A TR of 800 msec was optimal from theoretical calculations and proved optimal in control and tumor patients. Scans obtained with TR = 2000 msec, TE = 80 msec were inferior to short TR scans; such scans could fail to detect intracanalicular tumors. The relative resolving power in patients exceeded theoretical calculations because of greater than expected image contrast caused by low CSF signal intensity secondary to CSF pulsation.

Because there are numerous operator-dependent parameters in MR imaging, a number of publications have addressed the issue of optimizing pulse sequences for clinical scanning [1–5]. The question of an optimal pulse sequence requires specification of the clinical diagnostic problem before such a sequence can be defined. With the current and rapid development in instrumentation and imaging algorithms, this will certainly be an ongoing process.

The pulse sequence one chooses as optimal depends on the judgment criteria used. These criteria often relate to maximizing contrast differences, signal-to-noise ratio (SNR), or contrast-to-noise ratio [1–5]. Other factors have been used, such as constant scanning time [1]. The results generated by these methods differ because the criteria differ.

The complex interaction between SNR and contrast with long and short TR sequences, however, make single measurements such as SNR or contrast inadequate. A potentially useful measure of image diagnostic quality is "relative resolving power" (T). Resolving power is applicable when one is comparing detection ability of similarly sized objects. Resolving power has been discussed in the literature and recently has been modified and applied to MR [6–9]. It has the advantage of measuring more than one image parameter by considering three major components of image diagnostic quality: image contrast, SNR ratio, and spatial resolution. Resolving power differs from resolution in that the latter is an intrinsic characteristic of a scanner and is not object dependent. Resolving power is totally object dependent. Resolution of an MR scanner does not change with TR; resolving power does.

This paper discusses the application of relative resolving power to the specific clinical problem of optimizing detection of small tumors in the internal auditory canal (IAC) and in the cerebellopontine angle (CPA).

Received March 24, 1986; accepted after revision July 16, 1986.

Both authors: Department of Radiology, Stanford University School of Medicine, Stanford, CA 94305. Address reprint requests to D. R. Enzmann.

AJNR 8:99–106, January/February 1987
0195-6108/87/0801-0099

Materials and Methods

The primary purpose of this investigation was to determine the optimal TR (interpulse interval) for detecting small tumors in and around the IAC, most specifically intracanalicular and small acoustic neuromas situated at the porus acusticus. All patients were scanned (head coil) with a slick thickness of 3 mm with a gap of 0.6 mm (20%) between slices. The field of view (FOV) was 24 cm, resulting in a pixel size of 0.94 mm for a 256 × 256 matrix. In five patients smaller (20 and 16 cm) FOVs were studied, resulting in pixel sizes of 0.78 and 0.63 mm, respectively. In each patient, at least one of the following parameters was varied: TR at two or three settings and number of excitations (NEX) at either two or six. The NEX was varied only for short TR (400–1000 msec) sequences because of scanning time limitations. The following TRs were investigated: 400, 600, 800, 1000, and 2000 msec, each with an echo time (TE) of 25 msec. At TR = 2000 msec the following TEs were studied: 25, 40, and 80 msec. The data, therefore, allowed comparison of relative resolving power for different TRs and NEXs.

The patient population included 15 patients with tumors in the IAC or at the porus acusticus. These tumors varied from 6.0 mm to 2.0 cm in their greatest dimension. One of these patients had a facial neuroma, another a metastasis, and one had a small meningioma. The remainder were diagnosed as having acoustic neuromas, with seven confirmed surgically. Five patients have not had surgery but three have neurofibromatosis (one with bilateral tumors).

A control patient population was used to measure the relative resolving power of various pulse sequences for detecting 7th and 8th cranial nerve tumors. These controls consisted of 45 patients who had 3-mm slice-thickness scans for suspected posterior fossa pathology, but in whom no abnormality was detected.

Resolving power was initially defined by Rose [6], expanded on by Kaufman and Shosa [7, 8] and most recently applied to MR by Bradley et al. [9]. Resolving power is related to SNR, image contrast (C_i), and a confidence factor, k, which is defined as the number of standard deviations of noise between the signal and background; k typically falls in the range of 4–5 [6].

$$T = \frac{(SNR)^2 \times (C_i)^2}{k^2(1 + C_i + a/b)} \quad (1)$$

SNR = signal-to-noise ratio of the object; C_i = image contrast, a = area of object used to measure intensity, b = area of background used to measure intensity, and k = the confidence factor [6–9]. Our measurements were made in such a way that $a = b$. We were interested in the relative resolving power of different TRs. We divided all values by the T for TR = 400 msec, NEX = 2 pulse sequence to obtain the *relative* T. We arbitrarily set the T of TR = 400 msec, NEX = 2 at 100. In doing this, the confidence factor, k, was cancelled.

The SNR can be calculated from clinical magnitude images. With the GE Signa scanner, signal intensity is the measured intensity of the image minus 1024. Noise must be calculated because in a magnitude image it does not simply represent the standard deviation of air surrounding the head. The correct noise calculation is given by the following formula:

$$(\sigma_t)^2 = (\sigma_i)^2 + (N/N - 1)\ (\text{air intensity} - 1024)^2$$

σ_t = true standard deviation and σ_i = magnitude standard deviation of air in the image. N = the number of pixels used to measure air signal intensity. (See Appendix for derivation of this formula.)

The contrast term in equation (1) refers to image contrast (C_i) rather than object contrast (C_o). Image contrast is given by the following formula:

$$C_i = C_o \times e^{-\left(\frac{d}{D_1} \times \frac{d}{D_2}\right)} \quad (2)$$

C_i = image contrast, C_o = object contrast, D_1 = length of the object under study, D_2 = width of the object, and d = spatial resolution. Although spatial resolution for resolving power was defined as a full-width half-maximum value, the pixel size of the acquisition matrix is an adequate surrogate for this measure of resolution. D_1 and D_2 dimensions were used to account for nonspherical objects (i.e., the 7th and 8th cranial nerves). In this way a cylindrical object such as a tumor in the IAC can be modeled. Equation (2) holds true when d/D is less than 1.5 [7]. The d term was adjusted in resolving-power calculations for different acquisition matrixes (i.e., different pixel sizes). Object contrast (C_o) was defined as:

$$C_o = \frac{I_o - I_b}{I_b} \quad (3)$$

This is the usual definition, where I_o is object (lesion) signal intensity and Ib is background-tissue signal intensity. In these calculations background was CSF intensity. C_o differs from C_i (equation 2), which takes spatial resolution into account.

Theoretical calculations of SNR, image contrast, and relative resolving power for tumors and cranial nerves measuring 1 × 6 mm (D_1 = 1 mm, D_2 = 6 mm) were performed using the following equation and assumptions. Signal intensity was calculated from a partial saturation spin-echo sequence [10]:

$$I = N(H) \times (1 - 2e^{-(TR-TE/2)T1} + e^{-(TR/T1)}) \times e^{-TE/T2} \quad (4)$$

Reliable data on actual T1 and T2 measurements of acoustic neuromas (and meningiomas) at 1.5 T are not available. We chose, therefore, to model the difficult scenario in which the tumor had the same T1 and T2 relaxation times as gray matter. The tumor was assumed to have a proton density of 0.9, T1 = 800 msec, and T2 = 70 msec, similar to gray matter. This seemed reasonable given limited data. A T1 of meningioma has been reported between 500–600 msec at 0.15 T; we operated at 1.5 T. In our experience small acoustic neuromas have homogeneous signal intensity and do not have signal intensities significantly different from gray matter on short TR sequences (see illustrations where temporal lobe is visible). We emphasize small because our model was designed for the problems of detection posed by small neuromas. Larger lesions may have heterogeneous signal intensities and signal characteristics quite different from gray matter but their detection is usually not difficult. This is especially true of cystic lesions, which are generally large and do not represent the diagnostic challenge of the small intracanalicular tumors that we are trying to model. Nevertheless, a sensitivity analysis was carried out for tumor T1 values ranging from 800–1500 msec and for T2 ranging from 70–200 msec. CSF was assumed to have a proton density = 1, T1 = 2500 msec, and T2 = 250 msec [9]. These parameters were appropriate for the 1.5 T field strength system used.

To compare relative Ts of different TRs for the theoretical results, it was assumed that the SNR at TR = 400 msec was equal to 10. The actual SNR at TR = 400 msec measured in control patients was 9.2 (SD = 2.3) and 8.7 (SD = 0.7) in tumor patients. All SNR calculations and relative resolving-power calculations were referenced to a TR = 400 msec, NEX = 2 scan with pixel size = 0.94 mm, which arbitrarily was assigned T = 100. The theoretical calculations included three different pixel sizes, 0.94, 0.78, and 0.63 mm, representing three FOVs: 24, 20, and 16 cm. The dimensions D_1 and D_2 were run through a range of 0.1–10 mm to determine when it was optimal to decrease pixel size from 0.94 mm to 0.78 mm or lower.

Asymmetrical D_1 and D_2 values were used to simulate the 7th and 8th cranial nerves and IAC tumors and to determine any differences between spherical and nonspherical objects.

Relative T was calculated and grouped by TR for control patients and tumor patients. Signal intensity was measured using a region-of-interest (ROI) function on the scanner and subtracting 1024 from the mean of each measurement. Intensity values were measured within equal-size square ROIs confined within the tumor margins and CPA cistern, and within a strip of gray matter in the temporal lobe. The actual 7th and 8th cranial nerves were not used because at times the ROI box's minimum size included a partial volume of CSF. The temporal-lobe gray matter provided a more reliable measure. CSF measurements (same-size ROI) were taken in the CPA immediately next to the tumor or in the porus acusticus in control patients. Measurements of air included the mean, the standard deviation, and the number of pixels in the ROI. The latter two measurements were necessary for the corrected noise calculation (see Appendix). Air measurements were usually made in the lower right-hand corner of the image.

Results

Using gray matter as a surrogate for small acoustic neuromas (and meningiomas), the following calculated theoretical results were obtained. Figure 1 shows that for TE = 25 and NEX = 2 (one average) the maximum relative resolving power occurred at TR = 800 msec. Resolving power units were arbitrary with a TR = 400 msec, NEX = 2, and 0.94-mm pixel-size scan defined as 100. Reducing the pixel size of the acquisition matrix (i.e., increasing spatial resolution) generated a family of curves with the smaller pixel sizes having lower relative resolving power. The TR = 2000 msec, TE = 80 msec scan resulted in a relative T lower than a TR = 2000 msec, TE = 25 msec scan. Increasing NEX from two to six tripled the imaging time and, therefore, was only a reasonable strategy for short TR sequences. When this was done, the SNR increased by a factor of 1.71 and the relative T increased by a factor of 3, since SNR is squared in the resolving-power formula. Therefore, it is evident that increasing NEXs with short TR sequences significantly increased relative T compared with a long TR sequence, whereas the scanning time was nearly equivalent (Fig. 1). It was useful to calculate and graph the individual components of T, SNR, and C_i separately (Fig. 2). One can see the divergent effects of lengthening TR: the SNR increased while C_i contrast decreased. Given our assumptions, the problem posed by long TR sequences appeared to be low image contrast.

What if the assumptions are changed so the tumor T1 is longer? With T2 constant at 70 msec, the T1 can go to 1400 msec without changing the optimal TR. At longer T1s the optimal TR begins to decrease. By holding T1 constant at 800 msec but increasing T2 to 200 msec the optimal TR goes from 800 to 1000 msec. Clinically, T1 and T2 often increase in tandem so their effects counterbalance to some extent, but the optimal TR increases and falls in the 800–1100 msec range. As our tumor data showed, however, long T2s are not a feature of small acoustic neuromas. Longer T1s may occur but this has a minor effect on the optimal TR.

The relative T for gray matter measured in the control patient population showed curves similar to the theoretical curves (Figs. 1 and 3). This was to be expected since gray matter was used as the model tissue. With NEX = 2 and NEX = 6 the optimal TR was 800 msec. The difference between the NEX = 2 and NEX = 6 curves was greater than a factor of 3, predicted from the theoretical calculation (Figs. 1 and 3). The relative Ts of longer TEs (i.e., 40 and 80 msec) at TR = 2000 msec were lower than for short TR sequences with TE

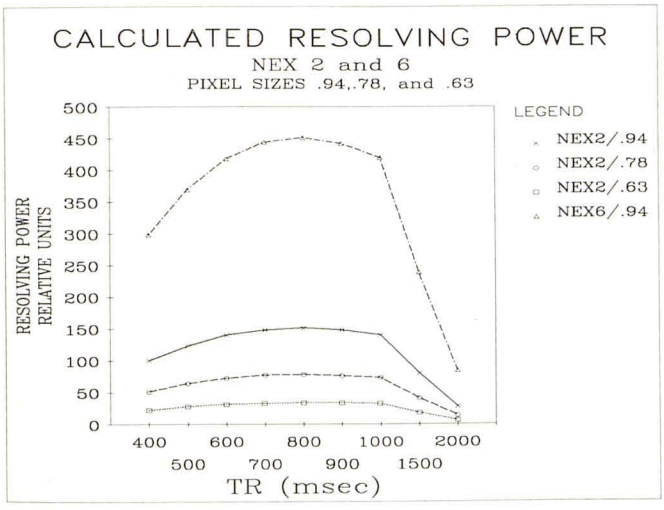

Fig. 1.—Theoretical relative resolving power for three different pixel sizes (0.94, 0.78, 0.63 mm) using two excitations (NEX). One curve shows effect on resolving power of increasing NEX to six excitations. TR = 400 msec and NEX = 2 scan with pixel size of 0.94 mm was assigned resolving power of 100; all other values are relative to this. Peak resolving power for all curves occurred at TR = 800 msec.

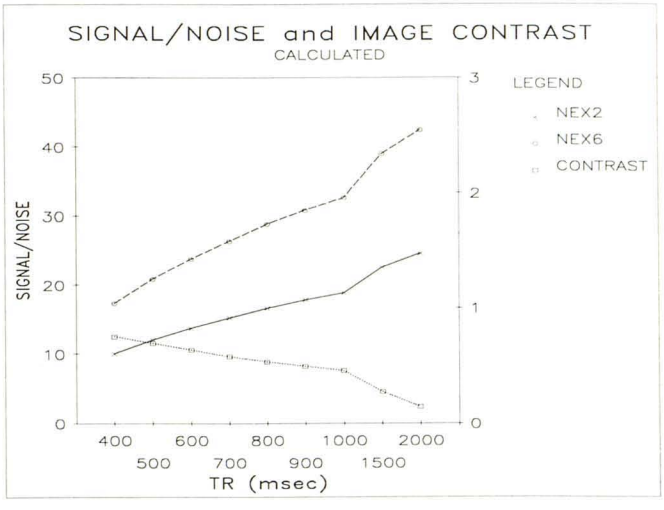

Fig. 2.—Resolving power was analyzed by its two major components: signal-to-noise ratio (SNR) (left y-axis) and image contrast (right y-axis). It was apparent that as TR increased, SNR increased while image contrast decreased. Note expected relationship between increased SNR and increasing NEX from 2 to 6.

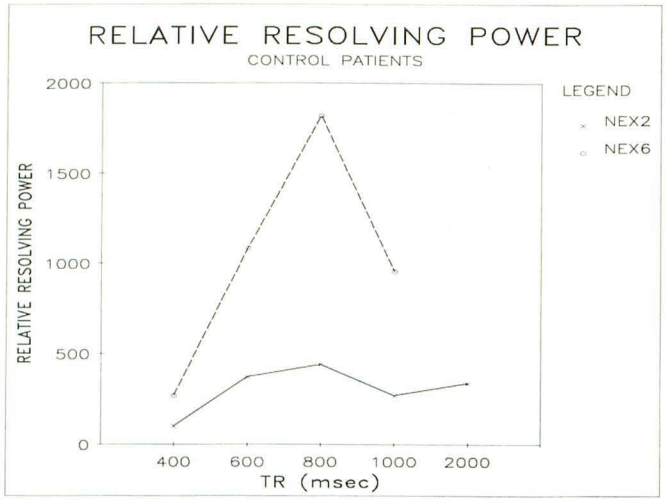

Fig. 3.—Relative resolving power in control patients using NEX = 2 and NEX = 6 sequences had a peak at TR = 800 msec. Note difference in scale of left y-axis compared with Fig. 1. Relative resolving power was greater than expected from theoretical calculations.

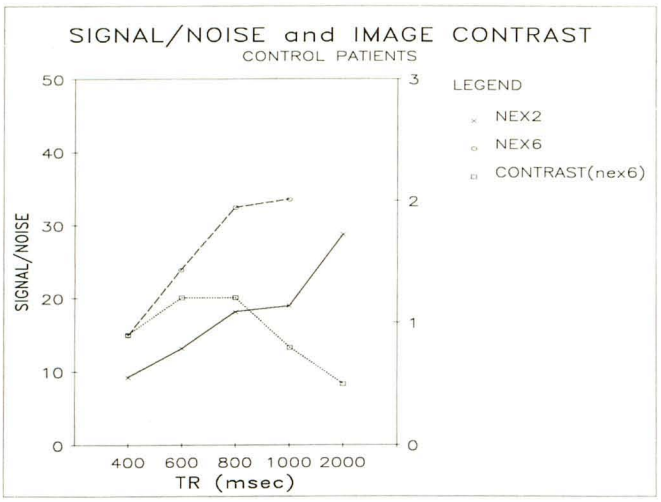

Fig. 4.—SNR and image-contrast curves for control patients. Image contrast increased to a plateau between TR = 600–800 msec and then decreased with higher TRs. As expected, SNR for NEX = 2 and NEX = 6 increased with longer TRs. SNR is on left y-axis; image contrast is on right y-axis.

= 25 msec. When relative T was analyzed by its SNR and C_i components (Fig. 4), the curves were again similar to the theoretical curves (Fig. 2). The SNR increased as TR lengthened. Image contrast, however, peaked in the TR = 600–800 msec range and then decreased as TR increased to 2000 msec (Fig. 4). The difference between the NEX = 2 and NEX = 6 SNR curves was as expected (Fig. 4).

The relative resolving power of small IAC and CPA tumors yielded curves that had both similarities and differences compared with the theoretical and control curves. The optimal TR for both NEX = 2 and NEX = 6 was 800 msec (Figs. 5 and 6). The magnitude of the relative T was distorted somewhat by an extremely high T in one patient. Without this, the curves would have been more similar. The other difference was the relatively good showing for TR = 2000 msec, TE = 25 msec in tumor patients (Fig. 5). This differed from the theoretical calculations (Fig. 1) and was better than in control patients (Fig. 3). The T2-weighted sequence of TR = 2000 msec, TE = 80 msec could, however, significantly hinder tumor detection (Fig. 6).

When SNR and C_i were considered separately, a similar pattern to that of control patients was seen. A peak in C_i was obtained at TR = 800 msec. Note that C_i at TR = 2000, TE = 25 in tumor patients (Fig. 7) was higher than in the control population (Fig. 4) and higher than expected from theoretical calculations (Fig. 2). The tumor patients, therefore, correlated closely with the pattern of relative Ts in the theoretical calculations and in control patients except for the higher level of C_i both at short (800 msec) and long (2000 msec) TRs. This increased contrast was due primarily to lower CSF signal intensity in tumor patients compared with control patients.

Three different pixel sizes of 0.94, 0.78, and 0.63 mm were investigated. The SNR decreased proportionately with pixel

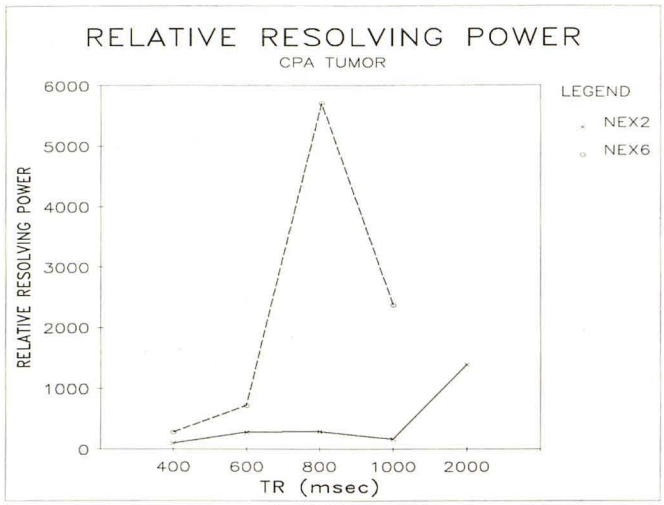

Fig. 5.—Relative resolving power of different sequences was greater in tumor patients. Note larger scale (y-axis) compared with Figs. 1 and 3. Peak resolving power for NEX = 2 and NEX = 6 occurred with TR = 800 msec. The large difference between these curves is explained in the text.

size as would be expected from the difference in voxel volume. This resultant loss in relative T for the tumor was readily apparent (Fig. 8). Theoretical calculations did not begin to favor a smaller pixel size of 0.78 over 0.94 mm until one dimension of the object fell below 0.7 mm while the other was above 1 mm, or until both dimensions reached 0.8 mm. With cylindrical objects the smallest dimension determined the optimal pixel size. The 0.94 mm pixel size proved useful in our system; a larger pixel size was not investigated.

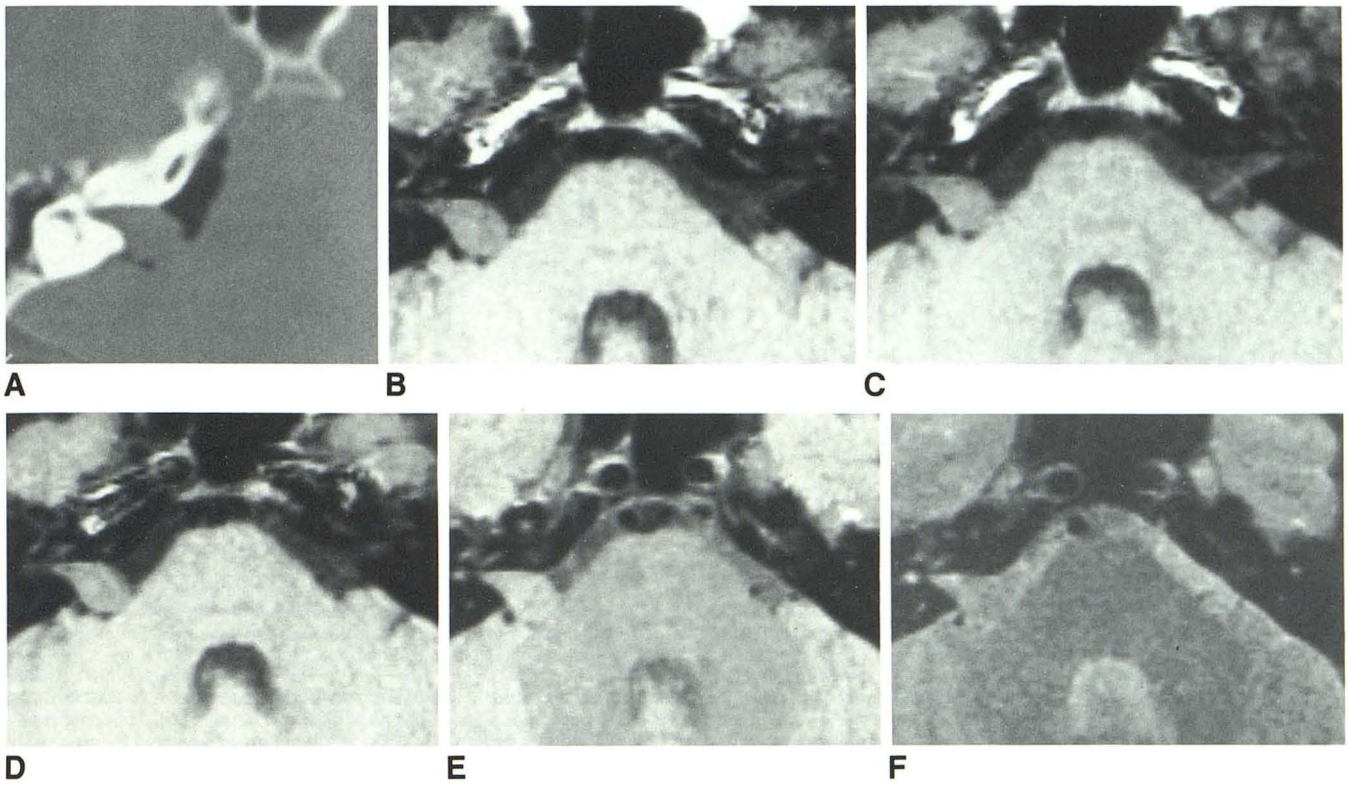

Fig. 6.—Scans of acoustic neuroma in 38-year-old man with neurofibromatosis show effect of varying TR on the detectability of 1 × 1.5 cm tumor. MR-scan findings correlated closely with appearance of tumor on CT-air cisternogram (*A*). Short TR sequences were performed as follows: *B*, TR = 400 msec, *C*, 600 msec, and *D*, 800 msec; slice thickness = 3 mm, field of view = 24 cm; matrix 256 × 256 (pixel size = 0.93 mm); and six excitations. Although tumor was seen well in all sequences, highest resolving power was calculated for TR = 800 msec scan (*D*). Long TR sequences of 2000 msec with TE = 25 msec (*E*) and 80 msec (*F*) were performed in same fashion except that two excitations were used. Loss of image contrast was apparent, especially on 80-msec echo image, making tumor difficult to detect (*F*). Tumor was detectable on 25-msec echo (*E*) but resolving power was less than on short TR sequences. Note that tumor signal intensity was virtually isointense with gray matter on both long and short TR sequences.

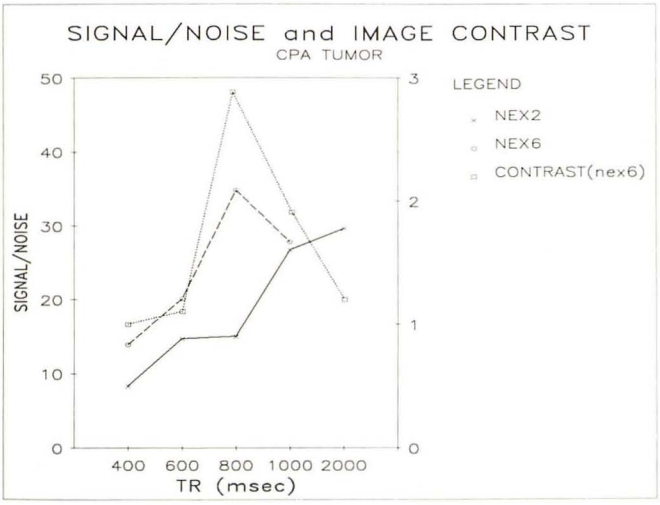

Fig. 7.—SNR and image-contrast curves for tumor patients. SNR curves were as expected except for drop-off at TR = 1000, NEX = 6. Image contrast peaked at TR = 800 msec and then decreased at longer TRs (right y-axis same as in Figs. 2 and 4). Magnitude of image contrast was higher than theoretical calculations or in control patients. This related to CSF pulsation discussed in text.

Discussion

Resolving power is a potentially useful tool for optimizing MR imaging pulse sequences. We used relative rather than absolute values of T because we were interested only in choosing the best of a number of alternative pulse sequences. Relative resolving power can be used to define and narrow the range of optimal pulse-sequence parameters for detecting a specific lesion. These parameters could then be tested clinically. As one might surmise and as our data showed, it is difficult to rely simply on SNR or contrast alone to optimize lesion detection. The interaction between SNR and contrast is complex; both image parameters need to be considered. Note how relative resolving power tied together parameters to define an optimum; parameters that, individually, did not really define an optimum TR.

The detection of small tumors in the IAC and CPA is an important clinical application of MR. MR has the ability to replace the CT-air cisternogram and become the definitive imaging test for the diagnosis of IAC tumors. For this reason, demanding yet realistic assumptions based on limited data were chosen to optimize the MR pulse sequence. Neuromas

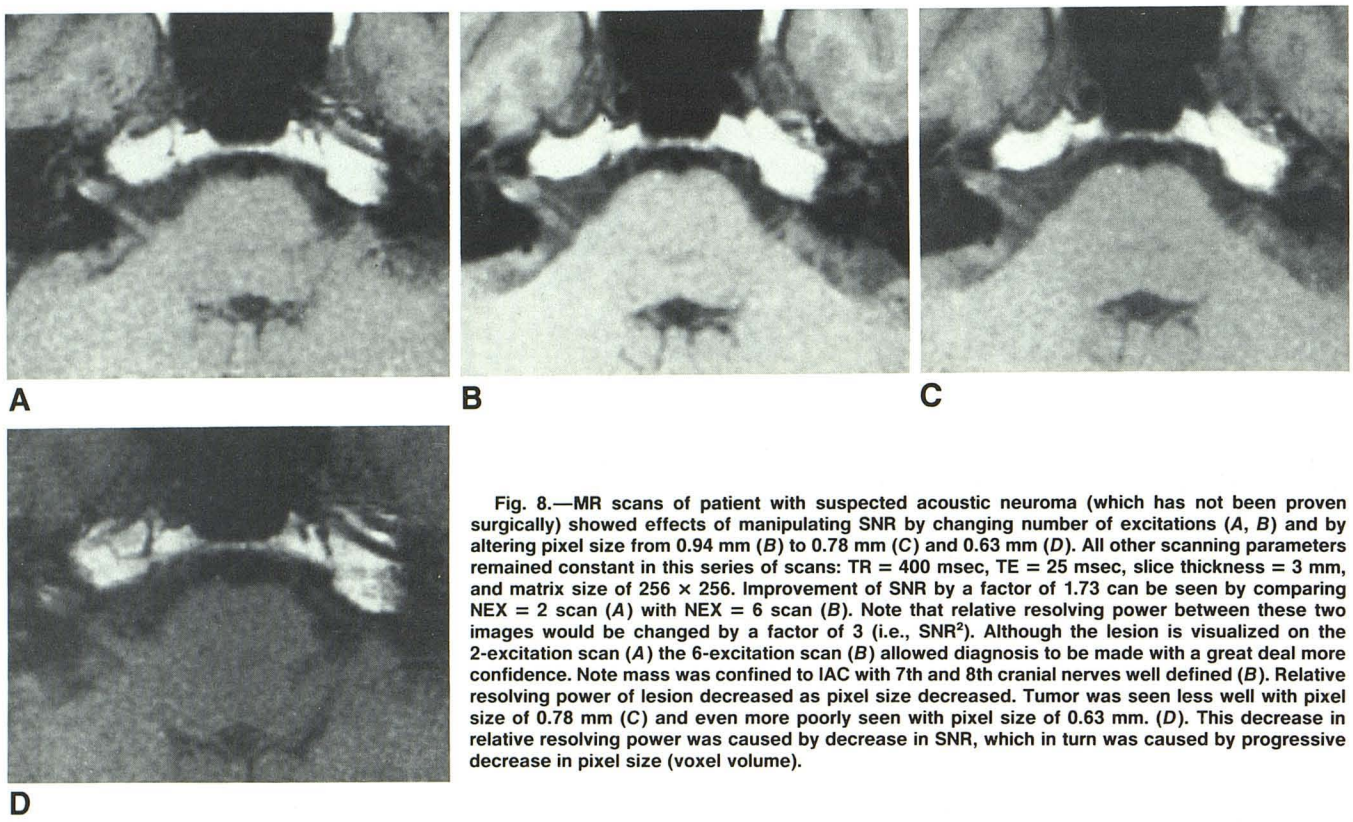

Fig. 8.—MR scans of patient with suspected acoustic neuroma (which has not been proven surgically) showed effects of manipulating SNR by changing number of excitations (*A*, *B*) and by altering pixel size from 0.94 mm (*B*) to 0.78 mm (*C*) and 0.63 mm (*D*). All other scanning parameters remained constant in this series of scans: TR = 400 msec, TE = 25 msec, slice thickness = 3 mm, and matrix size of 256 × 256. Improvement of SNR by a factor of 1.73 can be seen by comparing NEX = 2 scan (*A*) with NEX = 6 scan (*B*). Note that relative resolving power between these two images would be changed by a factor of 3 (i.e., SNR^2). Although the lesion is visualized on the 2-excitation scan (*A*) the 6-excitation scan (*B*) allowed diagnosis to be made with a great deal more confidence. Note mass was confined to IAC with 7th and 8th cranial nerves well defined (*B*). Relative resolving power of lesion decreased as pixel size decreased. Tumor was seen less well with pixel size of 0.78 mm (*C*) and even more poorly seen with pixel size of 0.63 mm. (*D*). This decrease in relative resolving power was caused by decrease in SNR, which in turn was caused by progressive decrease in pixel size (voxel volume).

and meningiomas in this region often behave similarly to adjacent brain in both their T1 and T2 characteristics [11–14]. This is especially true of small acoustic neuromas. Hence, our assumptions included tumor T1 and T2 characteristics similar to gray matter and a degree of spatial resolution necessary to resolve 1-mm structures (i.e., the normal 7th and 8th cranial nerves).

Given these assumptions, the calculated optimal TR at 1.5 T was 800 msec. This was confirmed by the actual tumor data. Theoretical calculations showed the optimal TR was relatively insensitive to the tumor's T1 and thus actual tumors could have had a wide range of T1s without altering the optimal TR. Significant variation in tumor T2s could have widened the range of optimal TRs but our tumor data did not show this. Long T2 relaxation times are not characteristic of small neuromas in the IAC. In light of the actual tumor data our initial assumptions appear to have been reasonable. A short TR optimum allows a strategy of increasing the number of excitations as a means of increasing SNR. Clinically, we found NEX = 6 a practical approach to increasing SNR, which permitted consistent identification of the cranial nerves.

These results differ somewhat from reports that have recommended other scanning parameters for acoustic neuroma [1, 9]. If we had focused on the SNR of a single tissue, then TR = 1000–1100 msec (1.4 × 800) would appear to be optimum [1]. This method examines only a single tissue, thereby ignoring the important variable of contrast with background tissue [1]. It also sets an arbitrary time limit, which is not a clinically useful point of view. Another study suggested a long TR of approximately 2000 msec, a TE = 26 msec, and a coarser matrix size in order to boost SNR [9]. This study used the petrous bone as the background tissue to measure contrast, whereas we feel the more appropriate and diagnostically important background is CSF. It is the CSF-tumor border that is crucial to the diagnosis of small IAC lesions rather than the interface with the petrous bone. The latter contrast is high whereas the contrast between tumor and CSF can be quite low and is more rate-limiting with respect to detection, especially with the long TR sequences. The choice of contrast measurement (tumor and bone) may explain the discrepancy in that report's recommendation of a long TR sequence as compared with our recommendation of a short TR sequence [8]. The theoretical calculations suggest that a relatively wide range of TRs will yield diagnostic images especially when six excitations are used. The clinical results suggest more of a peak at a TR = 800 msec with multiple excitations but the range of TR = 600–1000 appeared to be viable. Understanding the interplay between these parameters allows a choice of various options when patient motion or other time constraints become a clinical scanning problem.

Of the components that make up resolving power, SNR was an important factor in short TR scans. It could be increased with increasing NEXs. With longer TR scans, although SNR continued to rise, this beneficial effect became incrementally less. This positive effect on resolving power was also counterbalanced by a decrease in contrast, which became a detrimental factor in the higher TR range. This could not be overcome. Therefore, an increase in TR was beneficial as long as the SNR effect exceeded the reduction in contrast. Improving SNR by increasing NEX was not a

practical option with long TR scans. One could also increase SNR by increasing slice thickness from 3 to 5 mm. Our CT experience has shown that 3-mm slices are superior for evaluating the IAC because they minimize partial-thickness artifacts, but this concept may not necessarily hold with MR because tissue contrast is so different. One could increase the size of the voxel by using a 256 × 128 matrix to improve the SNR ratio, but that reduces the spatial resolution necessary for visualizing 1-mm nerves. SNR vs spatial resolution is a common clinical MR trade-off. It is inadvisable to sacrifice SNR for spatial resolution that is not needed clinically. The theoretical resolving-power calculations showed that spatial resolution greater than 0.94 mm pixel size was not necessary for IAC tumors unless lesions smaller than 1 mm were in question.

It is instructive to examine the formula for image contrast more closely (equation 3). For a given lesion size ($D_1 \times D_2$), decreasing the pixel size (d) improves image contrast. As the pixel size decreases, however, further incremental improvement in image contrast diminishes. This has to be balanced against the loss of SNR accompanying decreasing pixel (voxel) size. As the pixel size gets very small, SNR suffers severely while image contrast improves only marginally. In our theoretical calculations, moving from 0.94 mm to 0.78 and 0.63 mm pixel sizes did not improve resolving power for a lesion measuring 1 mm × 6 mm. The 1-mm dimension was the governing factor. When SNR becomes marginal, spatial resolution should be no greater than necessary for the desired true negative rate (i.e., specificity).

The relative Ts measured in tumor patients exceeded those of control patients and both of these were greater than the theoretical calculations. This was observed for both short and long TR sequences. What is the explanation for this? The formula (equation 4) used to calculate signal intensity for the partial saturation, spin-echo sequence, did not include a factor accounting for flow, specifically for CSF pulsatile flow. In a 3-mm slice through the CPA, CSF-flow phenomenon can have a profound effect on CSF signal intensity [15, 16]. Pulsation has the effect of decreasing CSF signal intensity, making it blacker [15, 16]. This increases image contrast for short and long TR sequences, where CSF would normally be white. This explains the higher than expected image contrast in control patients, especially in TR = 2000 msec images. The CSF-flow phenomenon seems to be accentuated by the presence of CPA and IAC tumors, thus increasing contrast even more. The degree of signal loss is proportional to CSF pulsation amplitude (velocity), which may be greater in tumor patients because their cisternal CSF spaces are narrower than normal [15, 16]. The CSF-flow phenomenon, however, also has a potential negative effect. It can cause a false positive TR = 2000 msec image for intracanalicular tumor because high signal from less mobile CSF within the IAC could be interpreted as tumor. The relatively stationary CSF within the IAC may seem bright compared with adjacent pulsatile CSF or the petrous bone and thus may simulate an intracanalicular tumor with a prolonged T2 [17]. A short TR sequence, however, should clear up any confusion. Our current protocol for suspected CPA and intracanalicular tumors is a long TR screening sequence (TR = 2000, TE = 25 and 80 msec, NEX = 1) to localize the IAC and to screen for other possible intracranial disease. This is followed by a TR = 800 msec sequence (TE = 25 msec) using six excitations to visualize the 7th and 8th cranial nerves and any potential tumor.

If MR is to serve as the definitive diagnostic test for small CPA and IAC tumors, it must match the air-CT cisternogram in sensitivity and, more importantly, in specificity. The true negative rate is of greater importance for a definitive test. False negative results make this expensive examination much less valuable in clinical practice. To achieve this role MR must accurately visualize the 7th and 8th cranial nerve bundles, whose thickness is approximately 1 mm in both the CPA cistern and the IAC. Small tumors of the same or lower signal intensity as the nerve bundles are the diagnostically limiting lesions. With a short TR scan, small tumor detection relies primarily on identifying anatomic distortion of the nerve-bundle complex. Larger lesions, which may have longer T2 relaxation times, are easier to detect and do not pose the risk of a false negative study. The larger lesions do not define the pulse sequence needed to minimize false negatives. At present, we do not feel that a contrast agent is required if adequate SNR is achievable with 1 mm spatial resolution [18].

Appendix

$$\sigma^2 = \frac{1}{N-1}\Sigma(p - \bar{p})^2$$

—zero baseline
—Noise level from zero baseline

$\bar{p}$ is in error because of magnitude image.
For the true σ, $\bar{p}_o$ is the true zero baseline.

$$\sigma_t^2 = \frac{1}{N-1}\Sigma(p - \bar{p}_o)^2$$

$$= \frac{1}{N-1}\{\Sigma p^2 - 2\Sigma p\bar{p}_o + \Sigma\bar{p}_o^2\}$$

But, $\bar{p}_o$ = zero in true case, so

$$\sigma_t^2 = \frac{1}{N-1}\Sigma p^2$$

$$\sigma^2 = \frac{1}{N-1}\{\Sigma p^2 - 2\Sigma p\bar{p} + \Sigma\bar{p}^2\}$$

$$(N-1)\sigma^2 = \Sigma p^2 - 2\bar{p}\Sigma p + \Sigma\bar{p}^2$$

$$= \Sigma p^2 - 2\bar{p}N\bar{p} + N\bar{p}^2$$

$$= \Sigma p^2 - N\bar{p}^2$$

$$\sigma^2 = \frac{1}{N-1}\Sigma p^2 - \frac{1}{N-1}\bar{p}^2$$

But, $\sigma_t^2 = \frac{1}{N-1}\Sigma p^2$. Therefore,

$$\sigma^2 = \sigma_t^2 - \frac{N}{N-1}\bar{p}^2$$

$$\sigma_t^2 = \sigma^2 + \frac{N}{N-1}\bar{p}^2$$

Note: By definition, S/N = $H/(\sigma_t)$. H = Signal height; and σ_t = true standard deviation.

ACKNOWLEDGMENT

We thank Leon Kaufman for his valuable input.

REFERENCES

1. Hendrick RE, Newman FD, Hendee WR. MR imaging technology: maximizing the signal-to-noise ratio from a single tissue. *Radiology* **1985**;156:749–752
2. Posin JP, Ortendahl DA, Hylton NM, et al. Variable magnetic resonance imaging parameters: effect on detection and characterization of lesions. *Radiology* **1985**;155:719–725
3. Ngo FQH, Bay JW, Kurland RJ, et al. Magnetic resonance of brain tumors: considerations of imaging contrast on the basis of relaxation measurements. *Mag Res Imaging* **1985**;3:145–155
4. Edelstein WA, Bottomley PA, Hart HR, Smith LS. Signal, noise, and contrast in nuclear magnetic resonance imaging. *J Comput Assist Tomogr* **1983;**7:391–401
5. Richardson ML, Amparo EG, Gillespy T, Helms CA, Demas BE, Genant HK. Theoretical considerations for optimizing intensity differences between primary musculoskeletal tumors and normal tissue with spin-echo magnetic resonance imaging. *Invest Radiol* **1985**;20:492–497
6. Rose AA. *Vision: human and electronic*. New York: Plenum, **1973**, 1–27
7. Kaufman L, Shosa D. Quantitative characterization of signal-to-noise ratios in diagnostic imaging instrumentation. In: Juge O, Donath A, eds. *Progress in Nuclear Medicine, Neuro-Nuclear Medicine*. Basel: Karger, **1981**, 1–17
8. Shosa D, Kaufman L. Methods for evaluation of diagnostic imaging instrumentation. *Phys Med Biol* **1981**;26:101–112
9. Bradley WG, Kortman KE, Crues JV. Central nervous system high-resolution magnetic resonance imaging: effect of increasing spatial resolution on resolving power. *Radiology* **1985**;156:93–98
10. Wehrli FW, MacFall JR, Shutts D, Breger R, Herfkens RJ. Mechanisms of contrast in NMR imaging. *J Comput Assist Tomogr* **1984**;8:369–380
11. Mikhael MA, Ciric IS, Wolff AP. Differentiation of cerebellopontine angle neuromas and meningiomas with MR imaging. *J Comput Assist Tomogr* **1985**;9:852–856
12. MacKay IM, Bydder GM, Young IR. MR imaging of central nervous system tumors that do not display increase in T1 or T2. *J Comput Assist Tomogr* **1985**;9:1055–1061
13. Bydder GM, Kingsley DPE, Niendorf HP, Young IR. MR imaging of meningiomas including studies with and without Gadolinium-DTPA. *J Comput Assist Tomogr* **1985**;9:690–697
14. McGinnis BD, Brady TJ, New PFJ, et al. Nuclear magnetic resonance (NMR) imaging of tumors in the posterior fossa. *J Comput Assist Tomogr* **1983;**7:575–584
15. Rubin JB, Enzmann DR. Imaging spinal CSF pulsation by 2DFT magnetic resonance: significance during clinical imaging. *ASNR Cornelius G. Dyke memorial award paper*, San Diego, CA, Jan **1986**
16. Rubin JB, Enzmann DR. Harmonic modulation of proton MR precessional phase by pulsatile motion: origin of spinal CSF flow phenomenon. *ASNR Cornelius G. Dyke memorial award paper*, San Diego, CA, Jan **1986**
17. Enzmann DR, Rubin JB, DeLaPaz R, Wright A. Benefits and pitfalls in MRI scanning resulting from CSF pulsation. *Radiology* **1986**; (in press)
18. Curati WL, Graif M, Kingsley DPE, Niendorf HP, Young IR. Acoustic neuromas: Gd-DTPA enhancement in MR imaging. *Radiology* **1986**;158:447–451